Journal of Materials Chemistry A

Accepted Manuscript

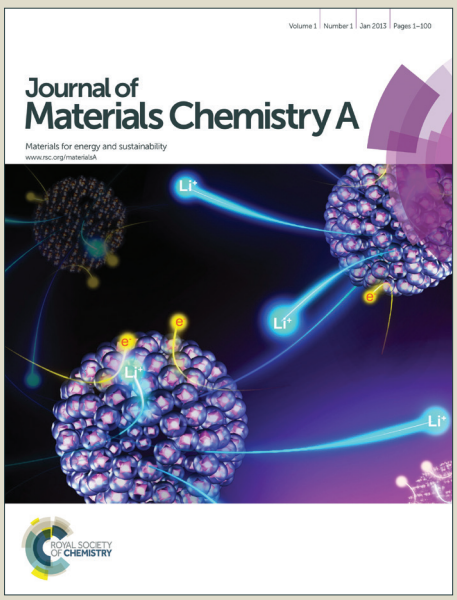

ROYAL SOCIETY OF CHEMISTRY

www.rsc.org/materialsA

Enhanced photocatalytic H_2 evolution over micro-SiC by coupling with CdS under visible light irradiation†

Yuan Peng, Zhongnan Guo, Jingjing Yang, Da Wang and Wenxia Yuan*

The rate of visible-light-driven photocatalytic hydrogen production from water splitting is intensively enhanced from zero to 555 μmol·h^{-1}·g^{-1} through hybridizing a proper amount of CdS particle onto micro-SiC surface. It suggests that the hybridization is responsible for lowering the surface activation energy of SiC and well-connected SiC/CdS interfaces serve as active sites for photocatalytic reactions, leading to this significant enhancement. The self-corrosion of CdS is simultaneously avoided and the composites show high stability. Our results demonstrate that SiC powder with high electron mobility, low cost, availability of large amount and environmental friendliness has a potential to become an efficient catalyst that might find practical applications.

Since the pioneering work by Fujishima and Honda in 1972,[1] compound semiconductors have become a major class of materials acting as photocatalysts for conversion of solar energy into hydrogen by splitting water.[2-7] By now, a number of criteria have been established to enhance the conversion efficiency for a semiconductor photocatalyst.[8-11] For instance, a suitable band gap required to absorb the sunlight energy as much as possible, a low recombination rate of photogenerated holes and electrons, good chemical stability to water corrosion, good crystallinity and so on. Semiconductor catalysts under investigation, however, seldom meet all above standards and exhibit desirable photocatalytic hydrogen evolution (PHE) activity.[12,13] Instead, they rarely outperform traditional TiO_2-based catalyst in conversion efficiency though the latter only utilizes 4% of sunlight energy owing to its wide band gap. The semiconductor materials with high solar-energy conversion efficiency that can be used practically for water splitting still need to be further explored.

Silicon carbide, a well-known semiconductor, is finding more and more applications in power electronics, light emitting diodes and radio frequency devices in the recent years due to its excellent electronic and thermal properties.[14-16] On the other hand, silicon carbide powder is one of the most useful abrasives in industry due to its hardness, low cost and environmental friendliness. This material has a band gap of 2.3-3.3 eV (which of β-SiC is 2.4 eV), and the bottom of its conduction band (CB) lies above the reduction potential of H^+ to H_2, which is more negative than CB of most semiconductors.[17-19] Silicon carbide should be an ideal visible-light-driven photocatalyst in terms of appropriate band gap and CB position. Moreover, its high charge-carrier mobility can offer an opportunity to quickly shuttle the photogenerated carriers before their recombination from the bulk to the surface of photocatalyst.[20] On the contrary, the SiC powder actually exhibits very weak photocatalytic activity, if any, under light illumination with wavelength from visible to ultraviolet range.[21,22] The solar water splitting, however, can occur over SiC if it is tailored into the forms of nano-sized particles, wires or rods or loading cocatalysts.[23-26] Our recent study verified that the water splitting proceeds only partially due to the photocatalytic activity of SiC, meanwhile, due to the direct reaction of the nano-sized SiC with water.[27] Hence, nano-sized SiC is not a good photocatalyst in this regard. More recently, it is found that photocatalytic performance of micro-sized SiC can be effectively activated and the PHE rate could reach 7.0 μmol·h^{-1} g^{-1} if 0.2 wt% Pt nanoparticle is added as a cocatalyst, which implies that the surface activation energy of SiC powder is too high or the number of active sites is too low to trigger the water splitting reaction. Considering SiC powder's rich availability and excellent semiconducting properties, it possess a potential to become an efficient catalyst that can find practical applications if the surface activation is tuned or improved through proper modification.

In this communication, a method of tuning the surface activation of the SiC powder via crystal engineering to create low surface activation energy spots is reported. We achieve this goal by hybridizing a proper amount of CdS grains, another semiconductor, onto SiC surface and well connected SiC/CdS interface form. As we know, CdS is a common photocatalyst and widely applied to combine with other semiconductors[28,29] because of its narrow band gap (2.4 eV) to absorb visible light and variable morphologies (nanowires[30], nanoparticles[31], quantum dots[32] and etc.) to be tuned by different methods. More importantly, the band edges of CdS are well matched with that of SiC and it is beneficial for the construction of effective Z-scheme system. Photocatalytic activity of SiC/CdS is significantly enhanced and the PHE activity reaches 555 $\mu mol \cdot h^{-1} g^{-1}$, a value even much higher than that of CdS. The PHE activity can be further increased up to 5460 $\mu mol \cdot h^{-1} g^{-1}$ if 3 wt% Pt was added. The self-corrosion of CdS is simultaneously avoided and the composites show high stability. The SiC-(CdS, Pt) contact interface is a crucial factor in ensuring a continuous electron flow between the source and target catalysts. Our work demonstrates that it is an effective route to induce and enhance the photocatalytic activity of SiC powder by lowering its surface activation energy. Practical SiC-based photocatalysts might be realized if another semiconductor with a well-matched band gap to SiC is found, which will be a focus of future research.

Mixtures of micro-SiC with CdS (SiC/CdS) were prepared by a facile wet chemistry method (see details in ESI†). The PHE activities of the prepared samples were evaluated by detecting hydrogen evolution from distilled water under visible-light illumination ($\lambda \geq 420$ nm) in the presence of Na_2S and Na_2SO_3 as sacrificial reagents. To assess the effectiveness of composite process, the X-ray diffraction patterns (XRD, Fig. S1a, ESI†) of SiC, CdS and SiC/CdS composites were compared. The results indicate that the composite consists of cubic phase CdS (ICDD-PDF No. 80-0019) and cubic-hexagonal mixed SiC (ICDD-PDF No. 29-1129 and 29-1131). After hybridization, diffraction peaks of individual SiC and CdS remain unchanged and no additional peaks are observed, which suggests that the hybrid process did not alter the crystal structures of the two semiconductors. The peaks of CdS become more obvious with the increasing content. No significant difference was observed in XRD patterns when loading Pt over SiC/CdS composite (mass ratio 1:0.5) (Fig. S1b, ESI†), which is probably due to the small amount and weak intensity.

Scanning electron microscope (SEM, Fig. S2, ESI†) was used to examine the morphologies of the as-prepared samples. The mean size of CdS grain is about 100 nm shown in Fig. S2a. For SiC/CdS composites (Fig. S2b-d), CdS attaches to the well-crystalized SiC particles. The close contact between the two materials can be observed in all three composites, whereas the coverage of the CdS on SiC particles is different. A large part of the SiC particles are still naked for SiC/CdS(1:0.2) composite in Fig. S2(b), while the one with 1:0.5 in Fig. S2c shows much larger coverage. When SiC/CdS ratio increased to 1:1 (see Fig. S2d), SiC particles are almost completely wrapped by CdS. It can be speculated that the best activity in this kind of composites depends on a proper content of two semiconductors.

Furthermore, transmission electron microscope (TEM) and high-resolution TEM (HRTEM) were applied to examine the structure of SiC/CdS-Pt composite (see Fig. 1a-c). The results show the close contact between SiC and CdS(Pt). HRTEM has a lattice spacing of ca. 0.336 nm, which can be assigned to the (111) lattice plane of CdS. The lattice fringe of ca. 0.226 nm of Pt was also observed on the CdS surface, which indicates Pt was loaded on CdS. Element mappings for Si, Cd, S and Pt in Fig. 1d and energy-dispersive X-ray spectroscopy (EDX, Fig. S3, ESI†) further confirms the presence of CdS and Pt on SiC.

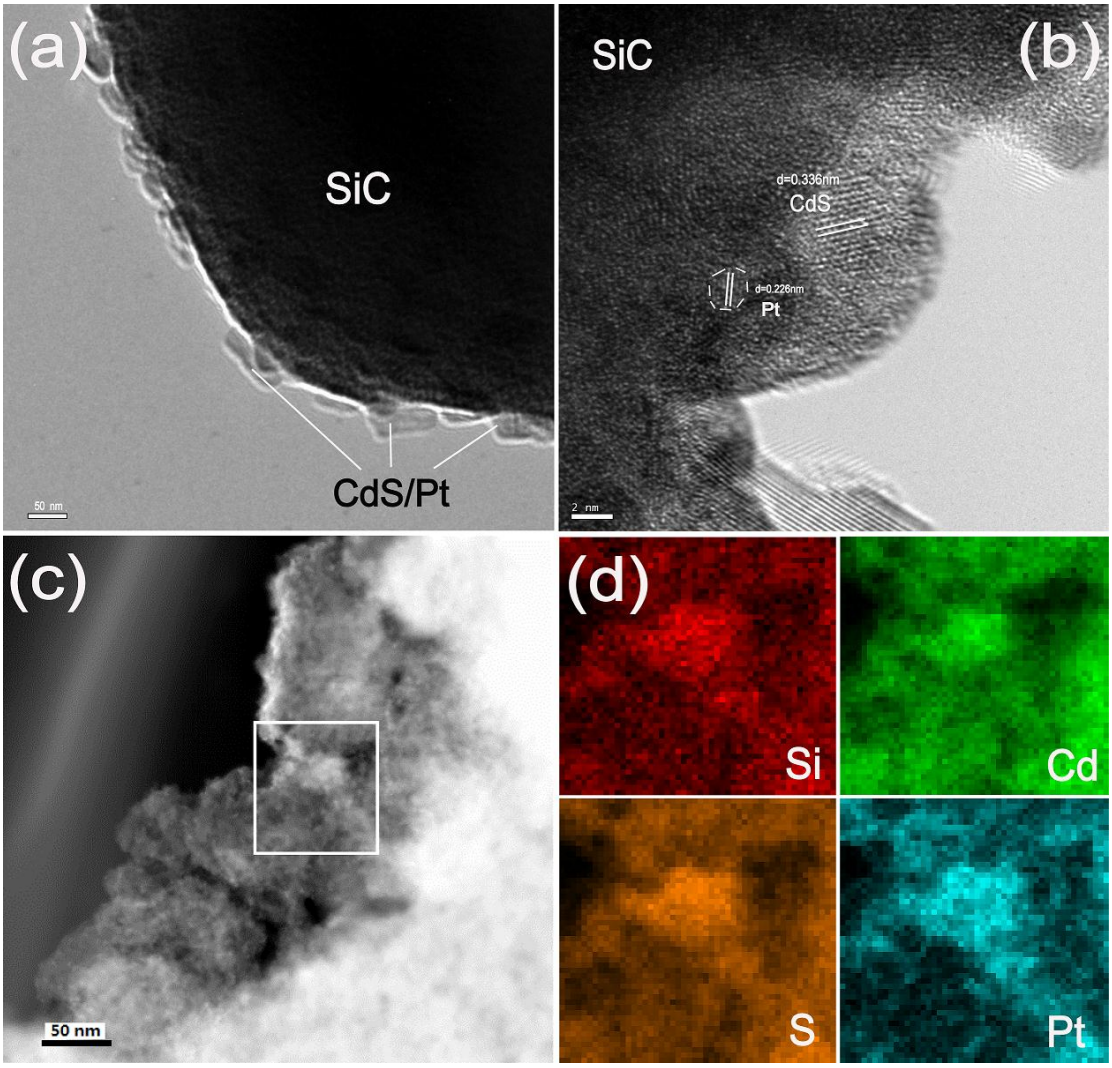

Fig. 1 TEM (a, c) and HRTEM (b) pictures of SiC/CdS- Pt composite and element mappings (d) of the boxed area in (c) for silicon, cadmium, sulfur, and platinum.

The hydrogen production of SiC, CdS, mechanically mixed SiC/CdS and the composites in 4 hours are shown in Fig. 2a. It can be seen that no appreciable H_2 evolution was detected over individual micro-SiC, and the PHE amount of pure CdS is 56 μmol H_2 in 4 h. In contrast, SiC/CdS composites all show high hydrogen amounts. In particular, SiC/CdS(1:0.5) composite exhibits the maximum hydrogen evolution of 111 μmol (equal to 555 $\mu mol \cdot h^{-1} \cdot g^{-1}$), which is 2 times of CdS. The apparent quantum efficiency (AQE) at the wavelength of 420 nm is 0.2%. The hydrogen production of SiC mechanically mixed with CdS with the mass ratio of 1:0.5 (denoted as Mix SiC/CdS(1:0.5)) was also measured and the result is comparable to that of CdS. In addition, cocatalyst Pt was photodeposited on SiC/CdS(1:0.5) composite and the PHE amounts and rates are illustrated in Fig. 2b-c. The optimal hydrogen evolution reaches 1091 μmol in 4 h (equal to 5460 $\mu mol \cdot h^{-1} \cdot g^{-1}$) with 3 wt% Pt, which is about 10 times than that of the one without loading. The AQE at 420 nm is 2.1%, which is about 40 times higher than previous one.[25] Furthermore, the photostability of SiC/CdS (1:0.5)-Pt catalyst was investigated (Fig. 2d) over 12 h, and the composite shows satisfactory stability during PHE reaction.

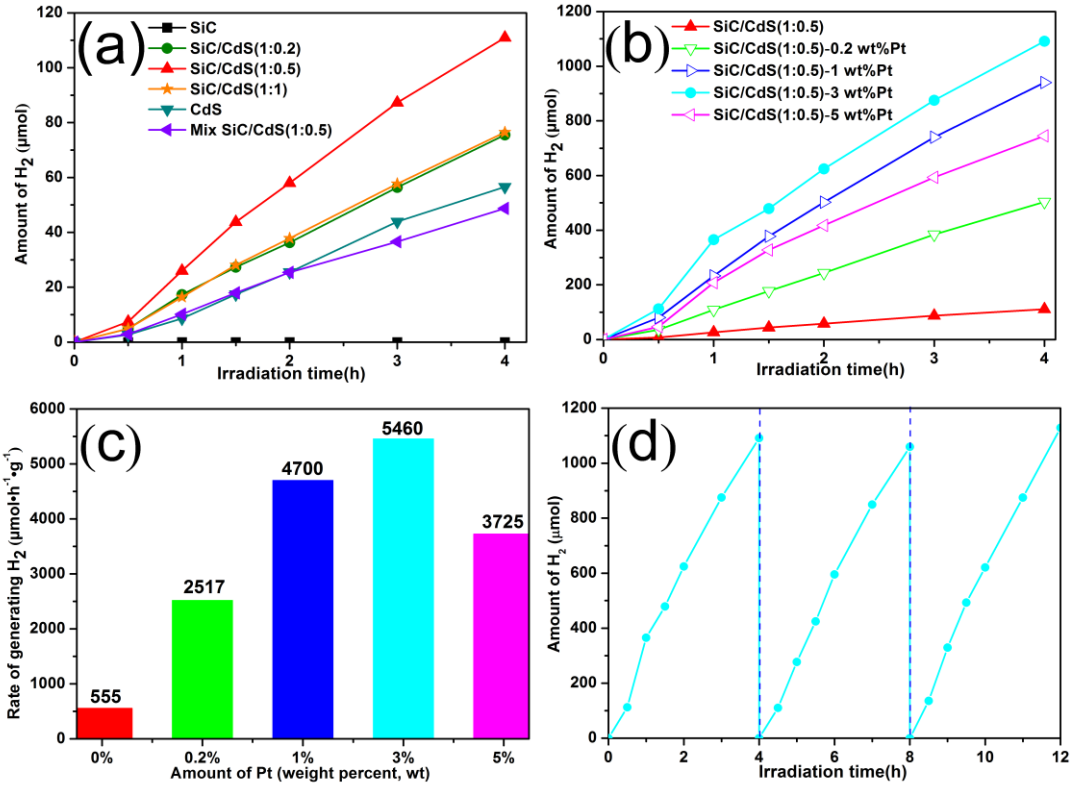

Fig. 2 PHE amounts of SiC, CdS, SiC/CdS composites and mechanically mixed SiC/CdS(1:0.5) (a); PHE amounts (b) and rates (c) of SiC/CdS(1:0.5)-*x*wt% Pt composites, *x* represents the weight percent of Pt; (d) Recycling test of SiC/CdS(1:0.5)-3 wt% Pt. Reaction condition: 50 mg photocatalysts were dispersed into 100 mL deionized water containing 0.1M Na_2S $9H_2O$ and 0.1M Na_2SO_3 as sacrificial reagents under visible light irradiation ($\lambda \geq 420$ nm).

Fig. 3a shows a comparison of UV-Vis diffuse reflection spectra (DRS) of the photocatalysts. It clearly demonstrates that SiC has a broad absorption in the ultraviolate and visible-light region. CdS displays a steep absorption in the visible-light range, showing the narrow size distribution of CdS nanocrystals. In comparison with SiC and CdS, apparent red-shifts towards the absorption edge can be seen in SiC/CdS composite, which indicates the composites have better light-harvesting ability. The digital photos of the samples (see Fig. S4, ESI†) demonstrate that their colors change from green of pure SiC to yellow of pure CdS with increasing amounts of CdS.

As we can see from Fig. 3a, the good light absorption of SiC indicates that it can be triggered by visible light. Nevertheless, the micro-SiC shows no appreciable hydrogen evolution amount (Fig. 2a), probably because its few active sites and high reaction barrier cause the fast electron-hole recombination. The speculation is confirmed by photoluminescence (PL) spectra in Fig. 3b. SiC exhibits the highest emission peak, which demonstrates that the electron-hole pairs in SiC bulk are easy to recombine with each other. The SiC/CdS composites show much lower emission intensities, especially for SiC/CdS(1:0.5). Meanwhile, loading cocatalyst Pt is also a benefit to decreasing excited electron-hole recombination further (Fig. 3b inset).

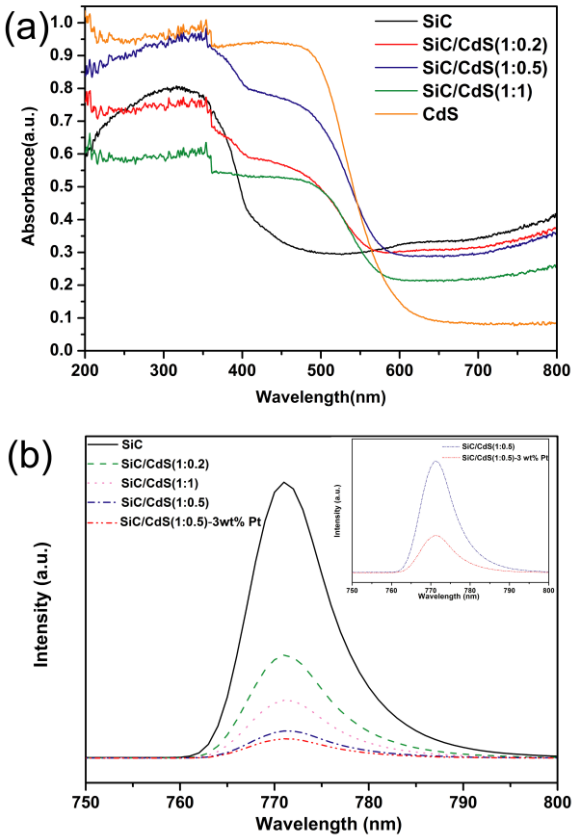

Fig. 3 DRS spectra (a) and PL spectra (b) of SiC, CdS and SiC/CdS composites.

When micro-SiC is coupled with CdS, the higher hydrogen evolution than SiC and CdS can be observed. The enhancement of PHE over SiC/CdS could be concluded as follows: First, the contact between SiC and CdS (Fig.1 and Fig. S2, ESI†) allows efficient carrier transfer at the interface. Second, with proper narrow band gaps of 2.4 eV,[8,17] both SiC and CdS can be excited by visible light. It is hopeful to generate more electrons and holes to participant in the PHE reactions. This can be indicated by the red-shift of the SiC/CdS composites in Fig. 3a. Third, the specific band edge positions of the CBs and valance bands (VBs) of SiC and CdS can be estimated by the following equation[33]

$$E_{CB} = \chi - E^e - \frac{1}{2} Eg \quad (1)$$

where E_{CB} is the CB edge potential. χ is the electronegativity of the semiconductor, expressed as the geometric mean of the absolute electronegativity of the constituent atoms, which is defined as the arithmetic mean of the atomic electron affinity and the first ionization energy. E^e is the energy of free electrons on the hydrogen scale ca. 4.5 eV. Eg is the band gap of the semiconductor. The calculated CB and VB of SiC are –0.23 and 2.17 eV, and those of CdS are –0.51 and 1.89 eV, respectively. So it is feasible to construct a direct Z-scheme between SiC and CdS. As we know, compared with traditional charge-carrier transfer process, direct Z-scheme is favorable for preserving photoexicited carriers with high energy, which is a benefit to photocatalysis in consideration of thermodynamic requirements.[34,35] It has been applied to efficient photocatalysis and the ability is higher than the individual ones.[36,37] In such a direct Z-scheme carrier transferring system, the photo-reduction and oxidation processes take place at different semiconductors, which it contributes to decrease the electron-hole recombination at the same time. This can be confirmed by lower emission intensities of the SiC/CdS composites (see Fig.3b). It

suggests that the active sites, in our case, should come from well-connected SiC/CdS interface, while Xing et al. illustrates that the oxidized Pt species embedded in the TiO_2 surface are the key active sites of Pt/TiO_2.[38]

It is worth noting that with the addition of CdS into the composite, the coverage rate of the CdS clusters on SiC particle is significantly different (Fig. S2(b-d)). When the CdS covering is relatively low, a large part of the SiC particles are still naked, which weakens the role of Z-scheme carrier system. While a moderate covering area guarantees the efficient carrier transfer. Contrarily, if SiC particles are completely wrapped by CdS cluster, the activity of the composite is getting lower. It can be considered that the light-absorbed ability of SiC was hampered by this excess-covering structure, which could also restrain the synergistic effect of the two semiconductors, resulting in a relatively low hydrogen evolution rate. Based on the photocatalytic activities of these two composites and pure SiC, it can be speculated that the ability of hydrogen evolution is mainly owing to an appropriate covering. The photocatalytic activity of SiC/CdS(1:0.5) reaches 555 $\mu mol \cdot h^{-1} \cdot g^{-1}$ (AQE 0.2%) under visible light, significantly higher than the previously-reported SiC-based photocatalysts.[21-26] In addition, the BET surface areas of SiC/CdS(1:0.5) (54 $m^2 \cdot g^{-1}$) is much higher than that of SiC (11 $m^2 \cdot g^{-1}$), which verifies that CdS increases the contact between photocatalys and water and offers active hydrogen-evolution sites in direct SiC/CdS Z-scheme. After loading Pt, the PHE amount increases to 10 times over the one without loading, Pt further contributes to accelerate separation and decrease recombination of electron-hole pairs.

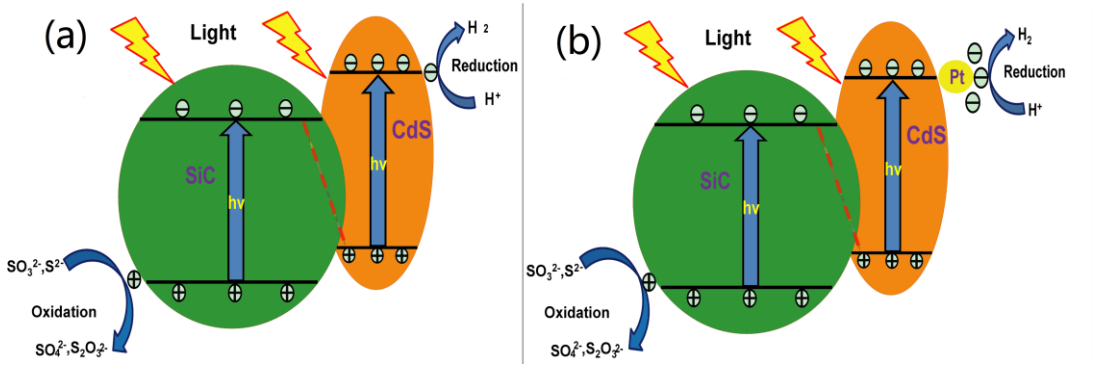

Fig. 4 Schematic illustrations of the mechanism over SiC/CdS composites (a) and SiC/CdS-Pt photocatalysts (b).

Fig. 4a shows a proposed mechanism of PHE over micro-SiC/CdS composite based on the direct Z-scheme. When individual SiC is triggered by visible light, the electrons and holes are prone to combine with each other for lack of surface active sites and driving force to separate. In contrast, when SiC is coupled with CdS, both SiC and CdS are excited by visible light to generate more electrons and holes. Additionally, close contact between SiC and CdS guarantees the electrons on the lower CB of SiC to be combined with the holes on higher VB of CdS at the interface. At the same time, the high-energy electrons on the higher CB of CdS accomplish the reduction process on the surface of CdS to generate H_2, and high-energy holes on the lower VB of SiC rapidly transfer to the surface of SiC to react with sacrificial reagents undergoing the oxidation process. In addition, it is because of the consumption of holes on the VB of CdS, its self-photocorrosion is also prevented and the stability of catalysts gets improved. Furthermore, cocatalyst Pt helps trap photoexcited electrons to generate H_2 and reduce the PHE potential, which makes the PHE amount increased further (Fig. 4b).

Conclusions

In summary, we have demonstrated that the visible-light-driven PHE ability from water splitting is intensively enhanced from zero to 555 $\mu mol \cdot h^{-1} \cdot g^{-1}$ through hybridizing a proper amount of CdS particles onto micro-SiC surfaces. The close contact between SiC and CdS provides a significant improvement in the activity for water

splitting by enhancing the light-utilization ability and efficiently separating photoexcited carriers. The loading of Pt particles over SiC/CdS composites further enhances PHE rate over 10 times than that without loading. This generate method is applicable to explore new and promising semiconductors to realize efficiently visible-light-driven photocatalytic water splitting.

Acknowledgements

The financial support by the National Natural Science Foundation of China (No. 50972010 and 51172025) and the Fundamental Research Funds for the Central Universities (FRF-TP-09-021B) are gratefully acknowledged.

Notes and references

Department of Chemistry, School of Chemistry and Biological Engineering, University of Science and Technology Beijing, Beijing 100083, China. E-mail: wenxiayuan20@aliyun.com; Fax:+ 86-010-62333033; Tel: +86-010-62332221

†Electronic Supplementary Information (ESI) available: Detailed experimental procedures and characterization results (XRD, SEM, EDX, digital pictures of samples). See DOI: 10.1039/c000000x/

1 A. Fujishima and K. Honda, *Nature*, 1972, **238**, 37.
2 H. Tada, T. Mitsui, T. Kiyonaga, T. Akita and K. Tanaka, *Nat. Mater.*, 2006, **5**, 782.
3 H. Park, W. Choi and M. R. Hoffmann, *J. Mater. Chem.*, 2008, **18**, 2379.
4 H. Yan, J. Yang, G. Ma, G. Wu, X. Zong, Z. Lei, J. Shi and C. Li, *J. Catal.*, 2009, **266**, 165.
5 Q. Xiang, J. Yu and M. Jaroniec, *J. Am. Chem. Soc.*, 2012, **134**, 6575.
6 W. Li, S. Xie, M. Li, X. Ouyang, G. Cui, X. Lu and Y. Tong, *J. Mater. Chem. A*, 2013, **1**, 4190.
7 Y. Jia, S. Shen, D. Wang, X. Wang, J. Shi, F. Zhang, H. Han and C. Li, *J. Mater. Chem. A*, 2013, **1**, 7905.
8 A. Kudo and Y. Miseki, *Chem. Soc. Rev.*, 2009, **38**, 253.
9 X. Chen, S. Shen, L. Guo and S. S. Mao, *Chem. Rev.*, 2010, **110**, 6503.
10 J. Xing, W. Q. Fang, H. J. Zhao and H. G. Yang, *Chem. Asian J.*, 2012, **7**, 642.
11 Y. Qu and X. Duan, *Chem. Soc. Rev.*, 2013, **42**, 2568.
12 T. Ohmori, H. Mametsuka and E. Suzuki, *Int. J. Hydrogen. Energy*, 2000, **25**, 953.
13 X. Wang, K. Maeda, A. Thomas, K. Takanabe, G. Xin, J. M. Carlsson, K. Domen and M. Antonietti, *Nat. Mater.*, 2008, **8**, 76.
14 R. M. Potter, J. M. Blank and A. Addamiano, *J. Appl. Phys.*, 1969, **40**, 2253.
15 M. Bhatnagar, P. K. McLarty and B. Baliga, *IEEE Electr. Device Lett.*, 1992, **13**, 501.
16 N. G. Wright, A. B. Horsfall and K. Vassilevski, *Mater. Today*, 2008, **11**, 16.
17 F. Wang, L. Zhang and Y. Zhang, *Nanoscale Res. Lett.*, 2009, **4**, 153.
18 V. Y. Aristov, *Physics-Uspekhi*, 2001, **44**, 761.
19 T. Inoue, A. Fujishima, S. Konishi and K. Honda, *Nature*, 1979, **277**, 637.
20 H. Matsunami and T. Kimoto, *Mat. Sci. Eng. R.*, 1997, **20**, 125.
21 Y. Nariki, Y. Inoue and K. Tanaka, *J. Mater. Sci.*, 1990, **25**, 3101.
22 Y. Gao, Y. Wang and Y. Wang, *React. Kinet. Catal. L.*, 2007, **91**, 13.
23 J. Hao, Y. Wang, X. Tong, G. Jin and X. Guo, *Int. J. Hydrogen. Energy*, 2012, **37**, 15038.
24 J. Hao, Y. Wang, X. Tong, G. Jin and X. Guo, *Catal. Today*, 2012, **212**, 220.
25 J. Yang, X. Zeng, L. Chen and W. Yuan, *Appl. Phys. Lett.*, 2013, **102**, 083101.
26 Y. Wang, X. Guo, L. Dong, G. Jin, Y. Wang and X. Guo, *Int. J. Hydrogen. Energy*, 2013, **38**, 12733.
27 J. Yang, Y. Yang, X. Zeng and W. Yuan, *Sci. Adv. Mater.*, 2013, **5**, 155.
28 J. Yu, J. Zhang and M. Jaroniec, *Green Chem.*, 2010, **12**, 1611.

29 L. Qi, J. Yu and M. Jaroniec, *Phys. Chem. Chem. Phys.*, 2011, **13**, 8915.

30 J. Jin, J. Yu, G. Liu and P. K. Wong, *J. Mater. Chem. A*, 2013, **1**, 10927.

31 P. Kundu, P. A. Deshpande, G. Madras and N. Ravishankar, *J. Mater. Chem.*, 2011, **21**, 4209.

32 X. Xing, R. Liu, X. Yu, G. Zhang, H. Cao, J. Yao, B. Ren, Z. Jiang and H. Zhao, *J. Mater. Chem. A*, 2013, **1**, 1488.

33 J. Zhang, J. Yu, Y. Zhang, Q. Li and J. R. Gong, *Nano Lett*, 2011, **11**, 4774.

34 X. Wang, G. Liu, Z. G. Chen, F. Li, L. Wang, G. Q. Lu and H. M. Cheng, *Chem. Commun.*, 2009, 3452.

35 Z. B. Yu, Y. P. Xie, G. Liu, G. Q. Lu, X. L. Ma and H. M. Cheng, *J. Mater. Chem. A*, 2013, **1**, 2773.

36 M. Miyauchi, Y. Nukui, D. Atarashi and E. Sakai, *ACS Appl. Mater. Inter.*, 2013, **5**, 9770.

37 J. Yu, S. Wang, J. Low and W. Xiao, *Phys. Chem. Chem. Phys.*, 2013, **15**, 16883.

38 J. Xing, H. Jiang, J. Chen, Y. Li, L. Wu, S. Yang, L. Zheng, H. Wang, P. Hu, H. Zhao and H. Yang, *J. Mater. Chem. A*, 2013, **1**, 15258.